Title

RNF4 interacts with both SUMO and nucleosomes to promote the DNA damage response

Journal

EMBO Reports, 15(5)

ISSN

1469-221X

Authors

Groocock, Lynda M

Nie, Minghua

Prudden, John

et al.

Publication Date

2014-05-01

DOI

10.1002/embr.201338369

Peer reviewed

Scientific Report

EMBO reports

RNF4 interacts with both SUMO and nucleosomes to promote the DNA damage response

Lynda M Groocock[1], Minghua Nie[1], John Prudden[1], Davide Moiani[2], Tao Wang[3], Anton Cheltsov[4], Robert P Rambo[5], Andrew S Arvai[2], Chiharu Hitomi[2], John A Tainer[2,5], Karolin Luger[3], J Jefferson P Perry[2,6,***], Eros Lazzerini-Denchi[7,**] & Michael N Boddy[1,*]

Abstract

The post-translational modification of DNA repair and checkpoint proteins by ubiquitin and small ubiquitin-like modifier (SUMO) critically orchestrates the DNA damage response (DDR). The ubiquitin ligase RNF4 integrates signaling by SUMO and ubiquitin, through its selective recognition and ubiquitination of SUMO-modified proteins. Here, we define a key new determinant for target discrimination by RNF4, in addition to interaction with SUMO. We identify a nucleosome-targeting motif within the RNF4 RING domain that can bind DNA and thereby enables RNF4 to selectively ubiquitinate nucleosomal histones. Furthermore, RNF4 nucleosome-targeting is crucially required for the repair of TRF2-depleted dysfunctional telomeres by 53BP1-mediated non-homologous end joining.

Keywords RNF4; SUMO-targeted E3 ubiquitin ligase (STUbL); small ubiquitin-like modifier; telomere; ubiquitin

Subject Categories DNA Replication, Repair & Recombination; Post-translational Modifications, Proteolysis & Proteomics

DOI 10.1002/embr.201338369 | Received 13 December 2013 | Revised 3 March 2014 | Accepted 4 March 2014 | Published online 8 April 2014

EMBO Reports (2014) 15: 601–608

Introduction

Post-translational protein modifications by ubiquitin and small ubiquitin-like modifier (SUMO) execute critical functions in orchestrating the DNA damage response (DDR) pathways at DNA double-strand breaks (DSBs) [1,2]. For example, the ubiquitin E3 ligases RNF8 and RNF168 polyubiquitinate histones H2A and H2AX [3,4], which like the sumoylation of DSB-associated substrates such as BRCA1 by the E3 SUMO ligases PIAS1 and PIAS4 [5,6], is a crucial component of the DDR to DSBs.

As at DSBs, ubiquitin signaling also plays a critical role in the cellular response to dysfunctional telomeres. Telomere function is ensured by a protein complex, termed shelterin, bound at telomeric DNA repeats [7–11]. A key shelterin constituent is the double-stranded DNA repeat-binding protein TRF2 [10]. Depletion of TRF2 activates an ATM-dependent DDR that leads to phosphorylation of the histone H2AX (γH2AX) and the serial recruitment of MDC1, RNF8, RNF168, 53BP1 and RIF1 [9,12–17]. Telomeres depleted for TRF2 become a substrate for the non-homologous end joining (NHEJ)-pathway leading to end-to-end chromosomal fusions [18]. In the absence of RNF8 or RNF168, 53BP1 cannot be recruited to telomeres, and NHEJ-mediated telomere fusions are severely impaired [14,16]. Although sumoylation by PIAS1/4 has not yet been implicated in the processing of dysfunctional telomeres, the Nse2 (MMS21) E3 SUMO ligase is required for the maintenance of telomere length by the "alternative lengthening of telomeres" (ALT) pathway in telomerase-deficient cancer cells [19].

How signaling through the SUMO and ubiquitin pathways is integrated to promote telomere repair is not known. The SUMO-targeted E3 ubiquitin ligase (STUbL) family of proteins mediates crosstalk between ubiquitin and SUMO. STUbL-dependent ubiquitination of SUMO conjugated target proteins, coupled or not with target degradation at the proteasome, drives key processes in the maintenance of genome stability [20–23]. The human STUbL RNF4 was recently demonstrated to act directly in DSB repair, by targeting multiple sumoylated proteins including MDC1, 53BP1 and BRCA1 [24–27].

1 Department of Cell and Molecular Biology, The Scripps Research Institute, La Jolla, CA, USA
2 Department of Integrative Structural and Computational Biology, The Scripps Research Institute, La Jolla, CA, USA
3 Department of Biochemistry and Molecular Biology, Howard Hughes Medical Institute, Colorado State University, Fort Collins, CO, USA
4 Q-MOL L.L.C., San Diego, CA, USA
5 Life Sciences Division, Lawrence Berkeley National Laboratory, Berkeley, CA, USA
6 Amrita School of Biotechnology, Amrita Vishwa Vidyapeetham, Amritapuri, Kollam, Kerala, India
7 Department of Molecular & Experimental Medicine, The Scripps Research Institute, La Jolla, CA, USA
*Corresponding author. Tel: +1 858 784 7042; Fax: +1 858 784 2265; E-mail: nboddy@scripps.edu
**Corresponding author. Tel: +1 858 784 7659; Fax: +1 858 784 8926; E-mail: edenchi@scripps.edu
***Corresponding author. Tel: +1 858 784 2284; Fax: +1 858 784 2277; E-mail: jjperry@scripps.edu

Herein, we demonstrate that RNF4 critically supports the ATM- and 53BP1-dependent NHEJ pathway that promotes the fusion of dysfunctional telomeres. Furthermore, we determine that in addition to its SUMO-interacting motifs (SIMs), RNF4 requires a previously undefined DNA binding and/or nucleosome-targeting motif within its RING domain to execute its DNA repair functions.

Results and Discussion

DNA binding by the RNF4 RING domain

Sequence analysis revealed a cluster of basic residues, R_{177}-K_{178}-K_{179}, adjacent to the human RNF4 RING domain C-terminal zinc-binding site, which is well conserved amongst homologs (Supplementary Fig S1). Like hRNF4, RNF168 and RING1b also contain this three residue basic cluster adjacent to their zinc-binding site (Fig 1A), while other RING-type E3 ubiquitin ligases do not (Supplementary Fig S1). Interestingly, this basic cluster supports nucleosome-specific ubiquitination of H2A by both RNF168 and RING1b, and additionally, DNA binding by RING1b [4,28].

We structurally determined human $RNF4_{120–190}$ RING domain by both in-solution small angle X-ray scattering (SAXS) and by protein crystallography to 2.0 Å resolution (4PPE.pdb; Supplementary Table S1). The latter provided a structure consistent to that previously determined (3NG2.pdb) and an indication of the quality of our recombinant material. Superimposition of the hRNF4 RING domain crystal structure with that of RING1b and RNF168 (PDB codes: 2CKL & 3L11) revealed a well-conserved architecture at the basic cluster region (Fig 1B). Rigid body-based docking analyses using DOT [29,30] of DNA oligonucleotides against both the entire hRNF4 crystal structure and against the entire RNF4:UbcH5:ubiquitin complex structure (PDB code: 4AP4; [31]) suggested a localized DNA binding site. These predicted interactions are centered at the RKK basic cluster, in addition to a neighboring set of basic residues, His_{182}-Lys_{183}-Arg_{184}, occurring in hRNF4 but not RING1b and RNF168 (Fig 1C and Supplementary Fig S2A). Using in-solution SAXS [32], we determined that hRNF4 RING domain forms a dimer in solution. Interestingly, the RNF4 structures with the C-terminus in a folded conformation, either *apo*-protein (PDB code 2XEU) or as observed in a complex with UbcH5:ubiquitin (4AP4), are a closer fit to the in-solution SAXS experimental data than RNF4 structures with the C-terminus in the extended conformation (Supplementary Fig S2). The in-solution folded C-terminus conformation of hRNF4 is consistent with previous studies indicating that this conformation is required for RNF4 activity [31]. We used the SAXS-based method MONSA that employs a multi-phase modeling to fit simultaneously multiple curves, and thus applies a contrast method to define interaction of protein and DNA constituents within the larger complex [33,34]. We collected SAXS data on apo-hRNF4 (Supplementary Fig S3), hRNF4 bound

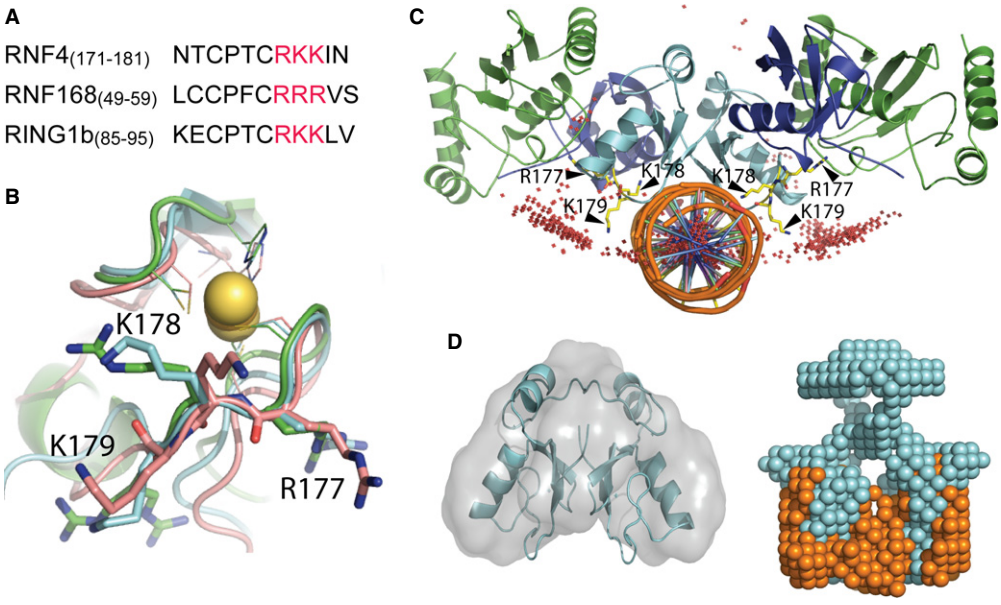

Figure 1. DNA binding motif within hRNF4 RING domain.

A Sequence alignment of human RNF4 RING domain with the homologous regions of RNF168 and RING1b.

B Structural superimposition of the basic RKK cluster of hRNF4 RING domain (cyan) with the homologous RRR cluster in RNF168 (green) and RING1b (salmon); zinc atoms are shown as gold spheres.

C DNA docking (DOT)-based molecular docking studies on the RNF4:UbcH5a:ubiquitin trimeric complex crystal structure (4AP4.pdb) with 12-bp DNA, RNF4 RING domains in cyan, ubiquitin in blue and UbcH5a E3 in green. The 2,000 most favorable interactions denoted by red spheres, with the R_{177}-K_{178}.K_{179} basic cluster in the C-terminus of the RNF4 RING domain highlighted in yellow, and top scoring dsDNA predictions depicted as cartoon images in orange.

D Left panel: GASBOR space fill model of the in-solution small angle X-ray scattering (SAXS) structure of *apo*-hRNF4, into which the hRNF4 RING crystal structure (2XEU.pdb) is fitted and illustrated as a cartoon diagram. Right panel: MONSA-based calculation of the in-solution SAXS shape of hRNF4 (cyan) in complex with a 12-bp dsDNA oligonucleotide (orange), depicted as dummy beads.

to a 12-bp double-stranded (ds) DNA oligonucleotide, and the 12-bp oligonucleotide alone (Supplementary Fig S4). The experimental SAXS curve of the hRNF4 RING domain in complex with 12-bp DNA versus the theoretical best linear combination of free DNA and free protein, revealed a distinct difference between these two plots (Supplementary Fig S4), indicating an interaction between the DNA and protein. MONSA provided a further clear indication that the protein and DNA components form an overall complex in solution that is in agreement with DOT-based predictions (Fig 1D).

We verified the DNA binding property of the hRNF4 RING *in vitro*, using a biotin-labeled DNA duplex immobilized on streptavidin beads. Compared to the Glutathione S-transferase (GST) control, hRNF4 RING bound well to the DNA duplex (Fig 2A). Our molecular docking analyses suggested that K179 within the RKK basic cluster directly interacts with DNA (Fig 1C). In agreement, both our hRNF4 structure and that of the RNF4:UbcH5:ubiquitin [31] complex show that K179 is solvent exposed and not involved in protein–protein interactions (Fig 1B). Strikingly, a point mutation, hRNF4-K179D, abolished the interaction between hRNF4 RING and DNA, which has a Kd of approximately 1 μM (Fig 2A, Supplementary Fig S5).

We next compared the activity of wild-type versus K179D mutant hRNF4 RING in an *in vitro* E3 ubiquitin ligase assay. Wild-type and K179D hRNF4 support similar kinetics of diubiquitin and polyubiquitin species formation, indicating that hRNF4-K179D retains full E3 ubiquitin ligase activity (Fig 2B and D, Supplementary Fig S5). Titration up to 150-fold molar excess of DNA over hRNF4 into the ubiquitination reaction demonstrated that DNA binding is neither activating nor inhibitory for hRNF4 (Fig 2C).

Together, the foregoing data show that the hRNF4 RING domain contains a non-specific DNA binding element related to that in the RING1b RING domain [28]. However, we note that DNA binding per se may not be the key function of the hRNF4 basic cluster, as it is structurally related to motifs in the RNF168 and RING1b RING domains that support nucleosome-targeting [4,28]. This structural homology has interesting implications for hRNF4 function in the DDR.

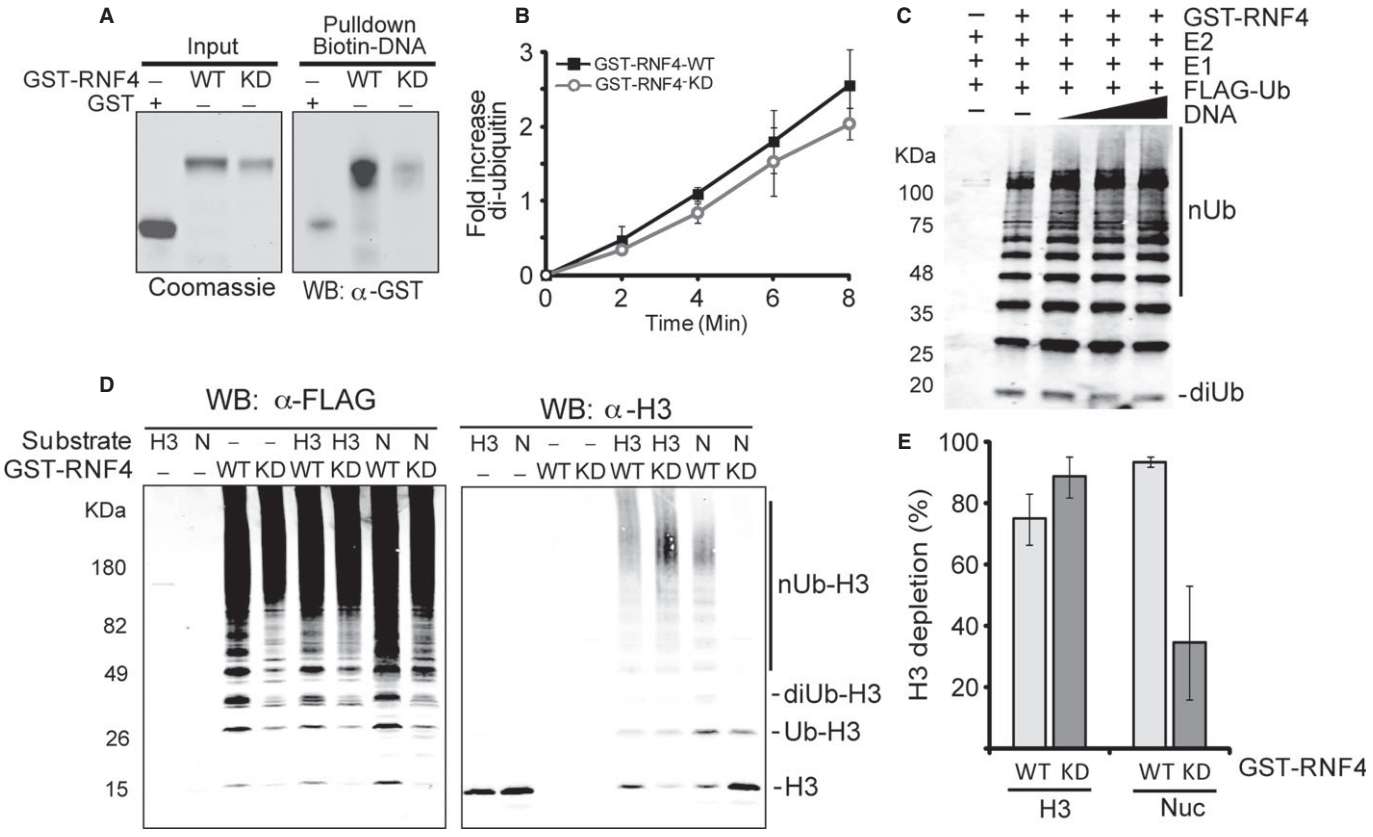

Figure 2. DNA binding and E3 Ligase activity of RNF4-K179D.

A GST-hRNF4 $RING_{120–190aa}$ domain purified using biotin-labeled duplex DNA, detected with an anti-GST antibody. Wild-type (WT) RNF4 RING domain, mutant K179D (KD) and free GST are shown.

B Kinetics of di-ubiquitin species formation by GST-RNF4. Mean and s.d. scored from triplicate experiments.

C Anti-FLAG western of *in vitro* ubiquitination assay in the presence of 12-bp duplex DNA titrated up to 150-fold molar excess relative to GST-RNF4 (0.2 μM).

D Anti-FLAG and anti-H3 western blot of *in vitro* ubiquitination of recombinant (H3) versus nucleosomal (N) histone H3 by wild-type (WT) and K179D mutant (KD) GST-RNF4 RING domain.

E Quantitation of unmodified H3 relative to free H3 and nucleosomal H3 input [lanes 1 and 2, respectively, in anti-H3 blot of (D)]. Mean and s.d. scored from triplicate experiments.

Nucleosome targeting supported by hRNF4 RING basic cluster

As both RNF168 and RING1b utilize their basic clusters to selectively modify histones within the nucleosomal context [4,28], we tested for similar functionality of hRNF4. Assayed against free histone, both wild-type and K179D hRNF4 strongly promoted H3 ubiquitination (Fig 2D and E). Notably however, whereas wild-type hRNF4 potently ubiquitinated H3 within assembled nucleosomes, the K179D mutant was strongly defective in this context (Fig 2D and E). Thus, the K179D mutation specifically attenuates the nucleosome-directed ubiquitin ligase activity of hRNF4. Importantly, the ability of hRNF4 to ubiquitinate nucleosomal H3 is mirrored by the ability of wild-type, but not K179D, to interact with nucleosomes in a gel shift assay (Supplementary Fig S5). As these nucleosomes lack linker DNA, the hRNF4 RING likely binds nucleosomal DNA and may optimally position hRNF4 to ubiquitinate H3. Overall, these results echo those for RNF168 and RING1b [4,28], indicating the existence of a small subfamily of RING-type E3 ubiquitin ligases that share a nucleosome-targeting motif.

A key role for RNF4 at dysfunctional telomeres

We next determined whether RNF4 plays a critical role at dysfunctional telomeres. To obtain complete and synchronous telomere deprotection, we used TRF2 conditional knockout mouse embryonic fibroblasts (MEFs) [13] that contain an inducible Cre recombinase (TRF2 Flox/Flox, Rosa26-Cre-ER; [35]). Following 4-hydroxy-tamoxifen (OHT) treatment, CRE-mediated recombination eliminates TRF2, thereby deprotecting chromosome ends.

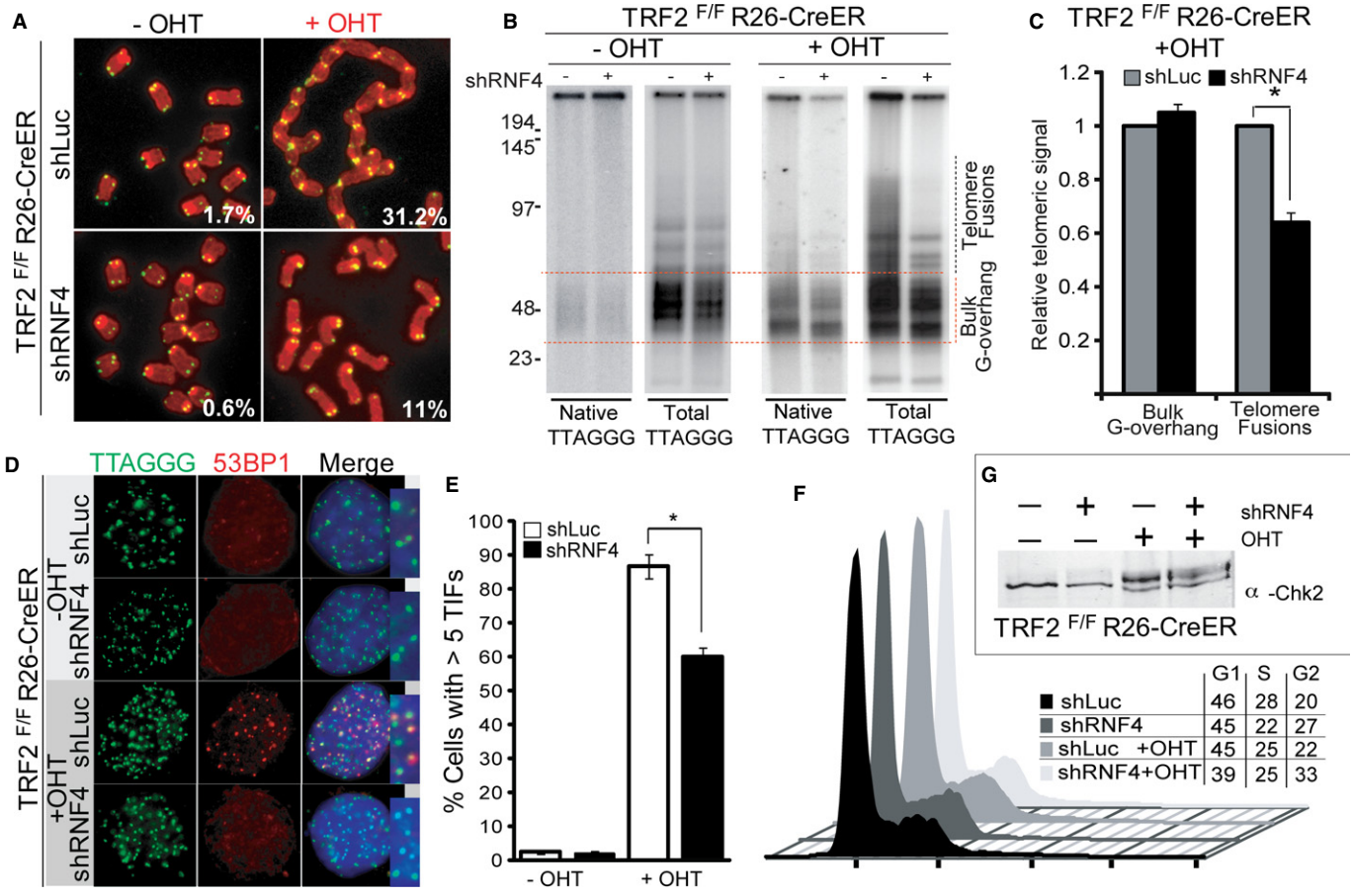

Figure 3. RNF4 is required for DNA damage response at telomeres.

A Metaphase spreads derived from mouse embryonic fibroblasts infected with the indicated constructs and either depleted for TRF2 (+OHT) or untreated (-OHT) were stained for telomeric DNA (green) and with DAPI (red). Percentages of fused chromosome ends are indicated.

B Telomeric restriction analysis performed on genomic DNA derived from cells treated as in (A). Hybridization in native conditions shows single-stranded telomeric DNA (Native). Hybridization following denaturation shows total telomeric DNA (Total).

C Quantitation of signal in (B); slow migrating fragments represent telomere end-to-end fusions and signal in native condition represents the single-stranded telomeric G-overhang. Mean and s.d. scored from triplicate experiments; $*P < 0.05$ as determined by two-tailed Student's *t*-test.

D Localization of 53BP1 to telomeric DNA (TTAGGG).

E Graph representing the percentage of cells with telomere dysfunction-induced foci (TIFs); Mean and s.d. scored from triplicate experiments, $n > 200$; $*P < 0.05$ as determined by two-tailed Student's *t*-test.

F FACS mediated cell cycle analysis of the indicated cells.

G ATM activation following TRF2 depletion as determined by Chk2 phosphorylation.

To test whether RNF4 plays a role in the DDR at TRF2-depleted telomeres, we reduced RNF4 expression by more than 90% using two independent lentiviral shRNA constructs (Supplementary Fig S6). Strikingly, metaphase spread analysis revealed that RNF4 is required for the formation of telomere fusions in TRF2-depleted cells (Fig 3A, Supplementary Table S2). This was confirmed in terminal restriction fragment analysis by the absence of slower migrating species that correspond to telomere fusions (Fig 3B and C). Given the pivotal role of 53BP1 in telomere fusion [13,18], we tested whether 53BP1 recruitment to dysfunctional telomeres was inhibited in RNF4-depleted cells. Indeed, attenuating RNF4 activity caused a significant reduction in 53BP1 co-localization with γH2AX in telomere dysfunction-induced foci (TIFs; Fig 3D and E, Supplementary Fig S7). These defects in telomere fusion and 53BP1 localization are not explained by changes in cell cycle profile in TRF2- and RNF4-depleted cells (Fig 3F); or a failure to activate the ATM pathway as assessed by CHK2 phosphorylation (Fig 3G). Moreover, the levels of γH2AX, MDC1, RNF168 and bulk ubiquitin conjugates (FK2) in TIFs at TRF2-depleted telomeres were similar in the presence or absence of RNF4 activity (Supplementary Fig S8). Interestingly, we detected a concurrent increase in the recruitment of BRCA1 into TIFs when RNF4 activity was compromised (Supplementary Fig S7). This result is consistent with the recent finding that 53BP1-binding protein RIF1 antagonizes recruitment of BRCA1 into TIFs [36].

hRNF4 nucleosome-targeting ability is critical to the telomeric DDR

We next tested whether RNF4's nucleosome-targeting activity is required for the DDR at dysfunctional telomeres by expressing sh-resistant RNF4 constructs in TRF2- and RNF4-depleted cells (Fig 4A). Cells expressing the RNF4-K179D mutant allele showed a strong defect in 53BP1 recruitment at telomeres (Fig 4B) and consistent with this, impaired NHEJ-mediated chromosome fusion (Fig 4C, Supplementary Table S2). A similar phenotype was observed in cells complemented with an empty vector or an RNF4 allele lacking its SUMO-interacting motifs (SIMs; Fig 4B and C). In contrast, expression of an sh-resistant wild-type RNF4 construct fully restored the ability of cells to process dysfunctional telomeres (Fig 4B and C). Together, these data indicate that both hRNF4 nucleosome-targeting ability and SIM-dependent SUMO recognition are required for the telomeric DDR.

RNF4 functions in the ATM-dependent DDR

The critical role for RNF4 at dysfunctional telomeres contrasts with its minor role at DNA DSBs induced by either ionizing radiation (IR) or laser irradiation [24–26]. Distinct from IR-induced DSBs that first evoke an ATM-dependent, and then rapidly following 5′–3′ DNA resection, an ATR-dependent response [37], TRF2 depletion activates the ATM- but not the ATR-dependent pathway [12]. We therefore speculated that RNF4 plays a crucial role in the ATM-dependent DDR, which we tested by depleting the telomere-associated protein TPP1 to trigger ATR but not ATM activation [12]. Interestingly, RNF4 activity was dispensable for the recruitment of 53BP1 at TPP1-depleted telomeres (Fig 5A and C, Supplementary Fig S9). These data indicate that RNF4 plays an important role in 53BP1 recruitment downstream of ATM, but is dispensable once ATR is activated.

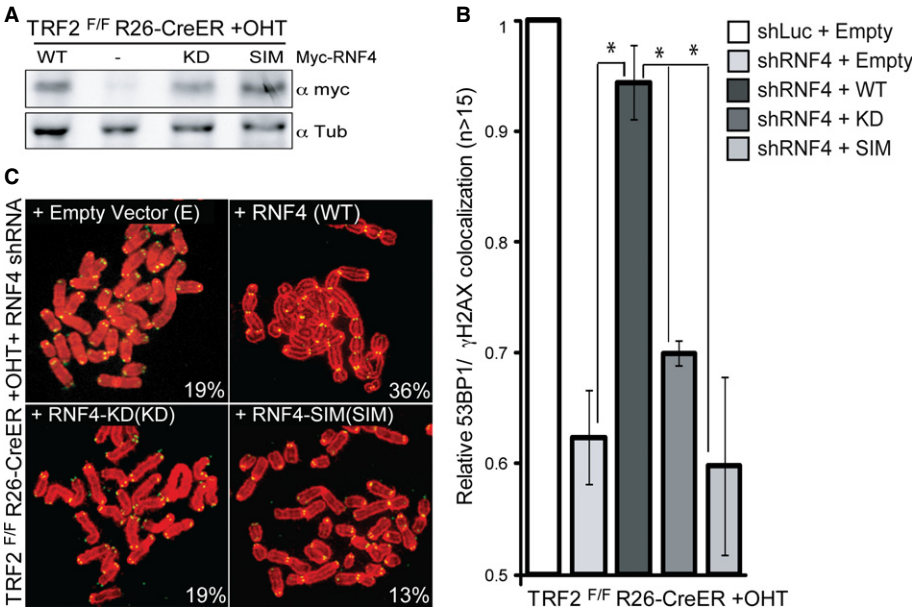

Figure 4. DNA binding activity of RNF4 is required for the DNA damage response.

A Expression levels of MYC-tagged RNF4 (WT) and RNF4 mutants [K179D (KD), SIM mutant (SIM)]. Tubulin (tub) was used as a loading control.

B TRF2 null cells depleted for endogenous RNF4 (shRNF4) were complemented with the indicated constructs and stained for γH2AX and 53BP1. The graph represents the proportion of cells with γH2AX and 53BP1 containing foci relative to control cells (shLuc). Mean and s.d. scored from triplicate experiments, $n > 200$; $^*P < 0.05$, calculated using a two-tailed Student's t-test.

C Metaphases harvested from cells treated as indicated were stained for telomeric DNA (green) and DAPI (red). Percentages of fused chromosome ends are indicated.

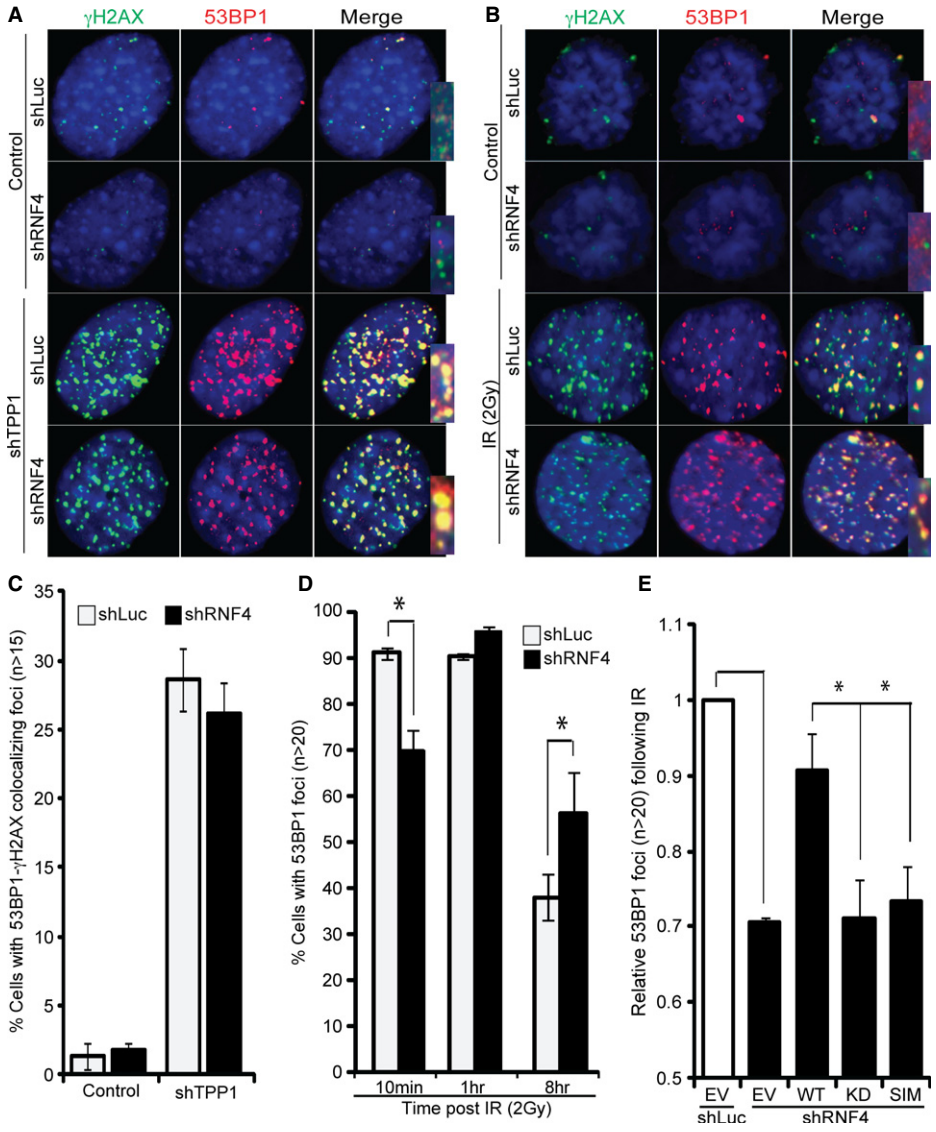

Figure 5. RNF4 acts downstream of ATM kinase signaling.

A Mouse embryonic fibroblasts (MEFs) infected with the indicated constructs were stained for γH2AX and 53BP1.

B MEFs infected with the indicated constructs were irradiated with 2 Gy and stained for 53BP1 and γH2AX.

C The graph represents the percentage of cells that display > 15 DNA damage foci containing 53BP1 and γH2AX. Mean and s.d. scored from triplicate experiments, $n > 200$.

D Quantitation of cells containing > 20 53BP1 foci at the indicated time post-ionizing radiation exposure. Mean and s.d. scored from triplicate experiments; $n > 200$; $^*P < 0.05$, calculated using a two-tailed Student's *t*-test.

E Quantitation of 53BP1 foci 10 min after irradiation (2 Gy) in MEFs expressing the indicated shRNA and RNF4 WT, K179D (KD), SIM mutant or empty vector (EV). Foci are normalized to mock treated cells with EV. Mean and s.d. scored from triplicate experiments; $n > 200$; $^*P < 0.05$, calculated using a two-tailed Students *t*-test.

We next determined whether the differential requirement for RNF4 in 53BP1 recruitment extended to global DSB repair, as opposed to reflecting a telomere specific role. To this end, we monitored the formation of 53BP1 DDR foci following IR at both early (ATM-dependent) and late (ATR-dependent) time points. RNF4 depletion caused a significant reduction in 53BP1 recruitment at early time points (~10 min), which was not apparent at later time points (Fig 5B and D). Thus, the ATM to ATR transition in the DDR likely explains the somewhat delayed but ultimately normal 53BP1 recruitment following IR treatment of RNF4-depleted cells (Fig 5B and D [26]).

The kinetic defect observed in 53BP1 recruitment to DSBs in RNF4-depleted cells provided an assay for any role of the RNF4 basic cluster in the DDR at DSBs. We tested whether RNF4-K179D was able to support the recruitment of 53BP1 into early IR-induced foci, by complementing RNF4-depleted MEFs with sh-resistant RNF4 constructs. Whereas wild-type RNF4 largely complemented the defect in 53BP1 recruitment into DDR foci, both the SIM and RNF4-K179D mutants were similarly deficient in this response (Fig 5E). Thus, the key role of the hRNF4 RING basic cluster in the telomeric DDR extends to its genome-wide DDR function.

Conclusions

Here, we have identified RNF4 as a key new player in the telomeric DDR, acting downstream of ATM to promote the recruitment of 53BP1 and subsequent NHEJ-mediated fusion of chromosomes. Furthermore, we have defined a basic cluster motif in the hRNF4 RING domain that is crucial for this DDR activity. The structural similarity of the hRNF4, RNF168 and RING1b basic clusters that enable selective ubiquitination of nucleosomal histones suggests intriguing functional parallels for these E3 ubiquitin ligases.

Our analyses support a minimally bipartite model for target discrimination by RNF4 in the DDR. The recognition of chromatin bound SUMO conjugates via its intrinsically disordered amino terminus acts as a primary "latch" for RNF4 recruitment [24,26]. Subsequently, we propose that the RNF4 RING domain can bind proximal chromatin to ubiquitinate nucleosomal histones and other chromatin-associated proteins to promote DNA repair (Supplementary Fig S9).

Materials and Methods

Cell culture, telomere analysis, Fluorescence-activated cell sorting

4-OHT treatment of $TRF2^{F/F}$, R26-CreER MEFs as well as lentiviral and retroviral infections were as previously described [35]. Cells were harvested 60 h post-addition of 4-OHT. Telomere Blots, fluorescence in situ hybridization, metaphase analysis and immunofluorescence (IF) were performed using existing protocols [13]. For quantification, at least 200 cells were counted following IF analysis. Cell cycle was determined by propidium iodide staining and acquired on a BD FACScalibur.

SAXS and crystallographic data collection/analysis

Small angle X-ray scattering data were collected at the SIBYLS beamline [38]. Data set on 15 μl sample volumes of purified hRNF4 RING domain. Initial SAXS data analyses were conducted with ScÅtter 2.0 software (https://bl1231.als.lbl.gov/scatter), and subsequently with the ATSAS software suite [39]. Standard data collection and processing protocols were used for the MONSA analysis, with data being collected on *apo*-RNF4, DNA oligonucleotide and RNF4 with DNA oligonucleotide, and shape reconstructions were conducted over multiple independent runs.

DNA docking

Docking calculations were performed using the global, systematic search program DOT, which is part of the DOT2 Suite distributed at: http://www.sdsc.edu/CCMS [29,40,41]. dsDNA of 10, 15 or 20 nt in length were used in the docking calculations. The 2,000 placements with the most favorable interaction energies, calculated as sum of electrostatics and van der Waals intermolecular energy terms, were kept, and the top 20 ranked hits were further analyzed in detail, with the aid of computer graphics. Further details including antibodies and primer sequences are available in Supplementary Materials and Methods.

Supplementary information for this article is available online: http://embor.embopress.org

Acknowledgements

M.N.B. is supported by a Scholar Award from the Leukemia & Lymphoma Society. This study was funded by NIH Grants GM068608 and GM081840 awarded to M.N.B., GM088409 to K.L., AR059968 to J.J.P.P., a Pew Scholars Award, the Novartis Advanced Discovery Institute and NIH grant AG038677 to E.L.D. X-ray scattering and diffraction technologies at the SIBYLS beamline (BL12.3.1) are funded by the IDAT program, supported by DOE Office of Biological and Environmental Research plus NIH Grants GM105404 and CA092584.

Author contributions

LMG conceived experiments and carried out the cell biology analyses, and JP performed the ubiquitination assays. MNB, ELD, JJPP and JAT conceived study, analyzed data and wrote manuscript. JJPP, ASA and CH performed protein structural and biophysical analyses. DM and AC performed docking studies. MN executed ubiquitination assays and ITC analyses. TW and KL provided nucleosomal substrates and advice on their use. RPR contributed to biophysical and SAXS data analyses.

Conflict of interest

The authors declare that they have no conflict of interest.

References

1. Morris JR (2010) More modifiers move on DNA damage. *Cancer Res* 70: 3861 – 3863
2. Bekker-Jensen S, Mailand N (2011) The ubiquitin- and SUMO-dependent signaling response to DNA double-strand breaks. *FEBS Lett* 585: 2914 – 2919
3. Stewart GS, Panier S, Townsend K, Al-Hakim AK, Kolas NK, Miller ES, Nakada S, Ylanko J, Olivarius S, Mendez M et al (2009) The RIDDLE syndrome protein mediates a ubiquitin-dependent signaling cascade at sites of DNA damage. *Cell* 136: 420 – 434
4. Mattiroli F, Vissers JH, van Dijk WJ, Ikpa P, Citterio E, Vermeulen W, Marteijn JA, Sixma TK (2012) RNF168 Ubiquitinates K13-15 on H2A/H2AX to Drive DNA Damage Signaling. *Cell* 150: 1182 – 1195
5. Galanty Y, Belotserkovskaya R, Coates J, Polo S, Miller KM, Jackson SP (2009) Mammalian SUMO E3-ligases PIAS1 and PIAS4 promote responses to DNA double-strand breaks. *Nature* 462: 935 – 939
6. Morris JR, Boutell C, Keppler M, Densham R, Weekes D, Alamshah A, Butler L, Galanty Y, Pangon L, Kiuchi T et al (2009) The SUMO modification pathway is involved in the BRCA1 response to genotoxic stress. *Nature* 462: 886 – 890
7. Artandi SE, DePinho RA (2000) A critical role for telomeres in suppressing and facilitating carcinogenesis. *Curr Opin Genet Dev* 10: 39 – 46
8. Blasco MA (2005) Telomeres and human disease: ageing, cancer and beyond. *Nat Rev Genet* 6: 611 – 622
9. Guo X, Deng Y, Lin Y, Cosme-Blanco W, Chan S, He H, Yuan G, Brown EJ, Chang S (2007) Dysfunctional telomeres activate an ATM-ATR-dependent DNA damage response to suppress tumorigenesis. *EMBO J* 26: 4709 – 4719
10. de Lange T (2005) Shelterin: the protein complex that shapes and safeguards human telomeres. *Genes Dev* 19: 2100 – 2110

11. De Lange T (2005) Telomere-related genome instability in cancer. *Cold Spring Harb Symp Quant Biol* 70: 197 – 204
12. Denchi EL, de Lange T (2007) Protection of telomeres through independent control of ATM and ATR by TRF2 and POT1. *Nature* 448: 1068 – 1071
13. Celli GB, de Lange T (2005) DNA processing is not required for ATM-mediated telomere damage response after TRF2 deletion. *Nat Cell Biol* 7: 712 – 718
14. Peuscher MH, Jacobs JJ (2011) DNA-damage response and repair activities at uncapped telomeres depend on RNF8. *Nat Cell Biol* 13: 1139 – 1145
15. Dimitrova N, de Lange T (2006) MDC1 accelerates nonhomologous end-joining of dysfunctional telomeres. *Genes Dev* 20: 3238 – 3243
16. Rai R, Li JM, Zheng H, Lok GT, Deng Y, Huen MS, Chen J, Jin J, Chang S (2011) The E3 ubiquitin ligase Rnf8 stabilizes Tpp1 to promote telomere end protection. *Nat Struct Mol Biol* 18: 1400 – 1407
17. Takai H, Smogorzewska A, de Lange T (2003) DNA damage foci at dysfunctional telomeres. *Curr Biol* 13: 1549 – 1556
18. Dimitrova N, Chen YC, Spector DL, de Lange T (2008) 53BP1 promotes non-homologous end joining of telomeres by increasing chromatin mobility. *Nature* 456: 524 – 528
19. Potts PR, Yu H (2007) The SMC5/6 complex maintains telomere length in ALT cancer cells through SUMOylation of telomere-binding proteins. *Nat Struct Mol Biol* 14: 581 – 590
20. Perry JJ, Tainer JA, Boddy MN (2008) A SIM-ultaneous role for SUMO and ubiquitin. *Trends Biochem Sci* 33: 201 – 208
21. Heideker J, Perry JJ, Boddy MN (2009) Genome stability roles of SUMO-targeted ubiquitin ligases. *DNA Repair (Amst.)* 8: 517 – 524
22. Hunter T, Sun H (2008) Crosstalk between the SUMO and ubiquitin pathways. *Ernst Schering Found Symp Proc* 1: 1 – 16
23. Sriramachandran AM, Dohmen RJ (2014) SUMO-targeted ubiquitin ligases. *Biochim Biophys Acta* 1843: 75 – 85
24. Galanty Y, Belotserkovskaya R, Coates J, Jackson SP (2012) RNF4, a SUMO-targeted ubiquitin E3 ligase, promotes DNA double-strand break repair. *Genes Dev* 26: 1179 – 1195
25. Luo K, Zhang H, Wang L, Yuan J, Lou Z (2012) Sumoylation of MDC1 is important for proper DNA damage response. *EMBO J* 31: 3008 – 3019
26. Yin Y, Seifert A, Chua JS, Maure JF, Golebiowski F, Hay RT (2012) SUMO-targeted ubiquitin E3 ligase RNF4 is required for the response of human cells to DNA damage. *Genes Dev* 26: 1196 – 1208
27. Vyas R, Kumar R, Clermont F, Helfricht A, Kalev P, Sotiropoulou P, Hendriks IA, Radaelli E, Hochepied T, Blanpain C et al (2013) RNF4 is required for DNA double-strand break repair in vivo. *Cell Death Differ* 20: 490 – 502
28. Bentley ML, Corn JE, Dong KC, Phung Q, Cheung TK, Cochran AG (2011) Recognition of UbcH5c and the nucleosome by the Bmi1/Ring1b ubiquitin ligase complex. *EMBO J* 30: 3285 – 3297
29. Roberts VA, Pique ME, Hsu S, Li S, Slupphaug G, Rambo RP, Jamison JW, Liu T, Lee JH, Tainer JA et al (2012) Combining H/D exchange mass spectroscopy and computational docking reveals extended DNA-binding surface on uracil-DNA glycosylase. *Nucleic Acids Res* 40: 6070 – 6081
30. Fan L, Roberts VA (2006) Complex of linker histone H5 with the nucleosome and its implications for chromatin packing. *Proc Natl Acad Sci USA* 103: 8384 – 8389
31. Plechanovova A, Jaffray EG, Tatham MH, Naismith JH, Hay RT (2012) Structure of a RING E3 ligase and ubiquitin-loaded E2 primed for catalysis. *Nature* 489: 115 – 120
32. Perry JJ, Tainer JA (2013) Developing advanced X-ray scattering methods combined with crystallography and computation. *Methods* 59: 363 – 371
33. Svergun DI (1999) Restoring low resolution structure of biological macromolecules from solution scattering using simulated annealing. *Biophys J* 76: 2879 – 2886
34. Svergun DI, Nierhaus KH (2000) A map of protein-rRNA distribution in the 70 S Escherichia coli ribosome. *J Biol Chem* 275: 14432 – 14439
35. Okamoto K, Bartocci C, Ouzounov I, Diedrich JK, Yates JR III, Denchi EL (2013) A two-step mechanism for TRF2-mediated chromosome-end protection. *Nature* 494: 502 – 505
36. Zimmermann M, Lottersberger F, Buonomo SB, Sfeir A, de Lange T (2013) 53BP1 regulates DSB repair using Rif1 to control 5′ end resection. *Science* 339: 700 – 704
37. Shiotani B, Zou L (2009) Single-stranded DNA orchestrates an ATM-to-ATR switch at DNA breaks. *Mol Cell* 33: 547 – 558
38. Classen S, Hura GL, Holton JM, Rambo RP, Rodic I, McGuire PJ, Dyer K, Hammel M, Meigs G, Frankel KA et al (2013) Implementation and performance of SIBYLS: a dual endstation small-angle X-ray scattering and macromolecular crystallography beamline at the advanced light source. *J Appl Crystallogr* 46: 1 – 13
39. Petoukhov MV, Konarev PV, Kikhney AG, Svergun D (2007) ATSAS 2.1—towards automated and web-supported small-angle scattering data analysis. *J Appl Crystallogr* 40: s223 – s228
40. Roberts VA, Pique ME (1999) Definition of the interaction domain for cytochrome c on cytochrome c oxidase. III. Prediction of the docked complex by a complete, systematic search. *J Biol Chem* 274: 38051 – 38060
41. Mandell JG, Roberts VA, Pique ME, Kotlovyi V, Mitchell JC, Nelson E, Tsigelny I, Ten Eyck LF (2001) Protein docking using continuum electrostatics and geometric fit. *Protein Eng* 14: 105 – 113

